Appl. Phys. A 82, 599–606 (2006)
DOI: 10.1007/s00339-005-3401-3

Applied Physics A
Materials Science & Processing

T. COTTINEAU[1]
M. TOUPIN[2]
T. DELAHAYE[1]
T. BROUSSE[1,2,✉]
D. BÉLANGER[2]

Nanostructured transition metal oxides for aqueous hybrid electrochemical supercapacitors

[1] Laboratoire de Génie des Matériaux, Ecole polytechnique de l'Université de Nantes, La Chantrerie, rue Christian Pauc, BP50609, 44306 Nantes Cedex 3, France
[2] Département de Chimie, Université du Québec à Montréal, Case Postale 8888, succursale Centre-Ville, Montréal, Québec, H3C 3P8, Canada

Received: 8 October 2004/Accepted: 17 August 2005
Published online: 1 November 2005 •

ABSTRACT In this paper, we wish to present an overview of the research carried out in our laboratories with low-cost transition metal oxides (manganese dioxide, iron oxide and vanadium oxide) as active electrode materials for aqueous electrochemical supercapacitors. More specifically, the paper focuses on the approaches that have been used to increase the capacitance of the metal oxides and the cell voltage of the supercapacitor. It is shown that the cell voltage of an electrochemical supercapacitor can be increased significantly with the use of hybrid systems. The most relevant associations are Fe_3O_4 or activated carbon as the negative electrode and MnO_2 as the positive. The cell voltage of the Fe_3O_4/MnO_2 device is 1.8 V and this value was increased to 2.2 V by using activated carbon instead of Fe_3O_4. These two systems have shown superior behavior compared to a symmetric MnO_2/MnO_2 device which only works within a 1 V potential window in aqueous K_2SO_4. Furthermore, the activated carbon/MnO_2 hybrid device exhibits a real power density of 605 W/kg (maximum power density = 19.0 kW/kg) with an energy density of 17.3 Wh/kg. These values compete well with those of standard electrochemical double layer capacitors working in organic electrolytes.

PACS 82.47.Uv; 82.45.Fk; 82.45.Yz

1 Introduction

Electrochemical supercapacitors are currently widely investigated due to their interesting characteristics in terms of power and energy densities. These power storage devices display much larger power densities than batteries and energy densities in comparison to conventional capacitors [1]. This makes them very attractive for applications requiring quick bursts of energy as is the case, for instance, for electronic devices. Electrochemical supercapacitors make use of three main classes of materials: (i) carbon [2–5], (ii) electronically conducting polymers [6–8] and (iii) metal oxides [1, 9–47]. The two last kinds of systems involve pseudo Faradaic reactions unlike carbon systems which use the double layer capacitance arising from the separation of charge at the interface between the solid electrode and an electrolyte.

✉ Fax: (33) 2 40 68 31 99,
E-mail: thierry.brousse@polytech.univ-nantes.fr

The most widely investigated metal oxide is unequivocally ruthenium oxide, which displays a fairly high specific capacitance (up to 700 F/g) but its use is severely limited by its high cost [9–11]. Consequently, alternative less costly materials were searched. In addition, recent research efforts were also aimed at using a more environmental friendly electrolyte than concentrated sulfuric acid. To this end, materials such as manganese oxide [12–39], iron oxide [28, 40–43], indium oxide [44], tin oxide [45] and vanadium oxide [46, 47] were synthesized and tested in presence of neutral electrolytic solution. These transition metal oxides were prepared as powder and use to prepare composite electrodes or directly deposited onto a conducting substrate.

The performance of an electrochemical supercapacitor, in terms of energy and power densities, is governed mainly by the specific capacitance of the active electrode materials and the cell voltage [1]. Obviously, the approach to improve the performance of a supercapacitor is to maximize both the capacitance and the cell voltage. The former is an intrinsic property of a material but it could be controlled by development of synthetic procedures that yield high surface area nanostructured metal oxides. On the other hand, the cell voltage is a critical parameter considering that it shows a square dependence with the energy and power densities and that it could be severely limited by the decomposition of water when aqueous electrolyte are used [48].

In this paper, we wish to present an overview of the research carried out in our laboratories with low-cost transition metal oxides as active materials for aqueous electrochemical supercapacitors [23, 28–30, 43, 47]. More specifically, the paper will focus on the approaches that have been used to increase the capacitance of the metal oxides and the cell voltage of the supercapacitor. It will be shown that the cell voltage of an electrochemical supercapacitor can be increased significantly with the use of hybrid systems [28, 29, 49]. This paper will focus on three different metal oxides: vanadium pentoxide, manganese dioxide, and magnetite.

2 Materials and methods

2.1 MnO_2 *synthesis*

The MnO_2 powder was synthesized via an adapted sol-gel route [50]. Briefly, fumaric acid ($C_4H_4O_4$, Aldrich) was added to $KMnO_4$ in a 1 : 3 molar ratio. After a few hours,

a black gel was formed. It was then carefully washed with 0.1 M H_2SO_4, deionized water, acetone and hexane respectively. The gel was dried in air for another 24 h. Alternatively, MnO_2 can be prepared by simple coprecipitation of $KMnO_4$ and $MnSO_4$ [12, 23, 30]. Both synthesis gives similar electrochemical performance.

2.2 Fe_3O_4 *synthesis*

Fe_3O_4 powder was prepared according to the synthesis reported by Zhou et al. [51]. Briefly, $FeSO_4 \cdot 7\,H_2O$ and $Fe(NO_3)_3 \cdot 9\,H_2O$ were dissolved in deoxygenated deionized water with a Fe(III)/Fe(II) molar ratio equal to 2. The solution was added dropwise to a 0.3 M NaOH solution vigorously stirred under N_2 bubbling. The resulting black precipitate was centrifuged at 5000 rpm, washed several times with deoxygenated water, and dried at 80 °C under moderate vacuum for 24 hours.

2.3 V_2O_5 *synthesis*

1 g of metallic vanadium powder was dissolved in 100 mL ice-cooled H_2O_2 (30%). After approximately 10 min, a vigorous evolution of oxygen started, due to the decomposition of excess H_2O_2. The solution then turned to a highly viscous dark brown sol, which was filtered, washed with deionized water and dried at 80 °C under moderate vacuum for 24 h [52].

2.4 *Chemical and structural analysis*

The crystallographic structure of the powder was investigated using a Siemens D-5000 X-ray diffractometer (Co K_α radiation, 0.179026 nm) in a $\theta/2\theta$ geometry. The microstructures of the samples were observed with a Leica Stereoscan 440 scanning electron microscope (SEM) coupled with an energy dispersive X-ray (EDX) analyzer (Oxford Instruments) for semi-quantitative analysis. Surface areas of the different oxides were measured by single point Brunauer-Emmett-Teller (BET) method with a Micromeritic Flowsorb II/2300 surface area analyzer using N_2 gas.

2.5 *Preparation of the electrodes*

Composite electrodes were prepared by mixing the active material (MnO_2, Fe_3O_4 or V_2O_5) with graphite (Alfa Aesar, conducting grade, −200 mesh), acetylene black (Alfa Aesar, > 99.9%, surface area = 80 m^2/g), and polytetrafluoroethylene (PTFE) dried powder in the following ratios: 70/12.5/12.5/5 for the MnO_2 positive electrode, 65/15/15/5 for the Fe_3O_4 and V_2O_5 negative electrodes and 90/5/0/5 for the carbon composite electrode. The mixtures thus prepared were cold rolled into 100 μm thick films. Pieces of film, typically 0.5 to 1 cm^2 size were then pressed at 900 MPa on a stainless steel grid connected to a copper wire.

Electrochemical tests were performed with a Solartron 1470 battery tester operated under Corrware II software (Scribner Associates). A Ag/AgCl (saturated NaCl) assembly and a platinum gauze were used as reference and counter electrodes, respectively. In this study, all electrodes were tested in 0.1 M K_2SO_4 solutions that were prepared by dissolving the appropriate amount of salt (K_2SO_4, Anachemia ACS) in deionized water without adjusting the pH which was about 6.8. The specific capacitance C (F/g) of a given composite electrode was determined by integrating the cyclic voltammogram curve to obtain the voltammetric charge (Q), and subsequently dividing this charge by the mass of the composite electrode (m) and the width of the potential window (ΔE),

$$C = Q/(\Delta E m) \tag{1}$$

The specific capacitance of the active material (MnO_2, Fe_3O_4 or V_2O_5) was calculated by dividing the specific capacitance of the composite electrode by the weight percentage of active material in this electrode. The influence of acetylene black (specific capacitance: 12 F/g) was taken into account in this last calculation.

The capacitors were built using two composite electrodes (typical surfaces: 0.5 to 1 cm^2) separated by a glass paper fiber wetted with 0.1 M K_2SO_4 solution. The three layers were then pressed in between two PTFE blocks (1 × 2 cm) by the mean of plastic clamps. The complete cell was immersed in 30 mL of 0.1 M K_2SO_4 in a glass vial without contact with ambient air. The cell was not thermostated; however, the ambient temperature was between 293 and 295 K.

The real power density, P_{real}, and the real energy, E_{real}, were determined from the constant current charge/discharge cycles as follows:

$$P_{\text{real}} = \Delta E I/m \text{ (W/kg)} \tag{2}$$

where $\Delta E = (E_{\max} + E_{\min})/2$ with $E_{\max}$ is the potential at the end of charge and $E_{\min}$ at the end of discharge, I the applied current (A) and m the weight of active material in the electrode (kg).

$$E_{\text{real}} = P_{\text{real}} t/3600 \text{ (Wh/kg)} \tag{3}$$

where t is the discharge time (s).

Alternatively, the maximum power density, which is the value commonly indicated for commercial devices, was calculated according to (4):

$$P_{\max} = (U_0^2)/(4Rm) \text{ (W/kg)} \tag{4}$$

where U_0 is the potential at the beginning of discharge (after the Ohmic drop) and R the internal resistance measured at 5 Hz (in Ω).

3 Results and discussions

3.1 *Morphology of the metal oxides*

Scanning electron micrographs of MnO_2, Fe_3O_4 and V_2O_5 are depicted in Fig. 1. The latter compound exhibits a fibrous microstructure whereas the morphology of MnO_2 and Fe_3O_4 mainly consists of nanosized grains (about 200 nm diameter) agglomerated in larger grains. The BET surface areas measured for MnO_2 and Fe_3O_4 (Table 1) are much larger than those expected from the geometric area calculated from the particle size. This suggests that the grains observed by

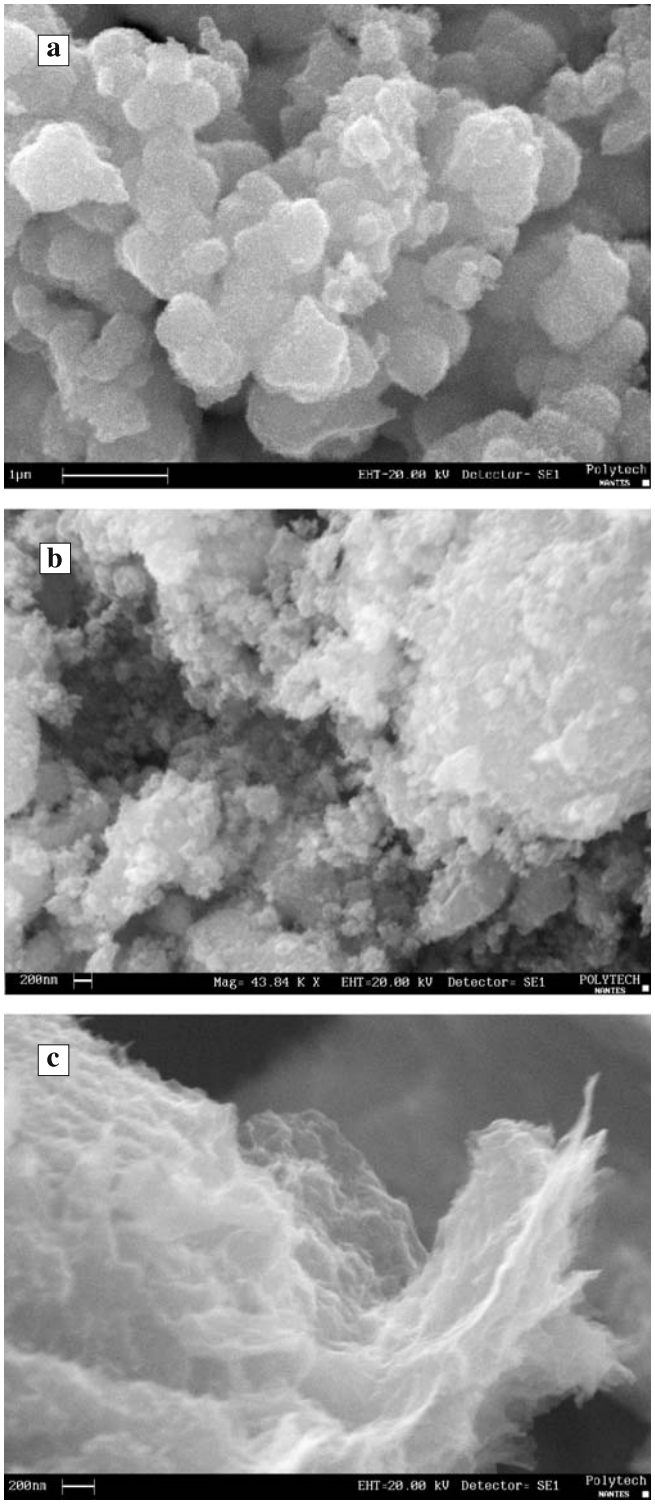

FIGURE 1 Scanning electron micrograph of (**a**) MnO_2, (**b**) Fe_3O_4 and (**c**) V_2O_5 powder (see experimental section for details of the synthesis procedures). *White bar* on the *bottom left corner* is 1 µm for (**a**) and 200 nm for (**b,c**)

SEM on Fig. 1 are porous or made of even smaller crystallites. MnO_2 and V_2O_5 show very broad diffraction peaks thus reflecting an amorphous structure, unlike Fe_3O_4, which exhibits large peaks which can be indexed according to magnetite (JCPDS 88-0315).

3.2 *Cyclic voltammetry (* CV*)*

The cyclic voltammograms of MnO_2, Fe_3O_4, V_2O_5 and carbon-based composite electrodes in aqueous electrolyte are presented in Fig. 2. It clearly shows that the potential window of each electrode materials differs significantly. The potential range for the MnO_2 (Fig. 2a) and V_2O_5 (Fig. 2c) electrodes extends from about −0.1 to 1.1 V and −0.4 to 1 V vs. Ag/AgCl, respectively, whereas the Fe_3O_4 electrode (Fig. 2b) is stable at more negative potentials. The potential window over which an electrode material can be cycled is thermodynamically limited by the hydrogen and oxygen evolution reactions, which occur at −0.56 and 0.67 V vs. Ag/AgCl, respectively for a pH close to 7 [48]. However, more negative (for reduction) and positive (for oxidation) potentials can be reached since both the hydrogen and oxygen evolution reactions are presumably kinetically limited on these oxides and carbon electrodes. This is obviously the case for the MnO_2 electrode, which does not show any visible evidence for gas formation at a potential as high as 1 V [12–39]. The same is true for the Fe_3O_4 and the carbon electrode at the negative potential limit and for these electrode materials the negative limit can be set at about −0.7 and −1.2 V, respectively [40–43]. For the activated carbon electrode, the potential window might appear wide, however, the onset of Faradaic processes (e.g., oxygen evolution reaction) can be detected above 0.6 V vs. Ag/AgCl, which makes this material less useful than MnO_2 as a positive electrode in an hybrid aqueous cell. Additionally, some redox waves attributed to oxygenated surface groups can be clearly observed on the CV at about 0.4 V vs. Ag/AgCl [3]. Another parameter of crucial importance that governs the useful potential range of an electrode material is the potential for which dissolution or decomposition of the active electrode material occurs. For the oxides investigated in this work, these phenomena are evidenced by a coloration of the electrolyte upon cycling for too much positive or negative potentials. For example, when a Fe_3O_4 electrode is cycled at potential more negative than −0.8 V, a well defined redox wave is observed with a peak potential of −1.1 V (not shown) and is also accompanied by a loss of capacitance. The nature of this redox process is unclear but Fe_3O_4 should be reduced to metallic Fe in these conditions [48].

A close look at the shape of the cyclic voltammograms presented in Fig. 2a reveals that, among the oxides, only MnO_2 presents a quasi-rectangular shape close to that expected for a pure electrochemical double layer capacitor, even if Faradaic processes dominate the electrochemical behavior of MnO_2 electrode in K_2SO_4 [30]. For the two other oxides, Fe_3O_4 and V_2O_5, the Faradaic character is clearly indicated by broad oxidative and reductive waves on the cyclic voltammogram (Fig. 2b and c). A detailed investigation concerning the redox processes of these two oxides is currently underway and the results will be presented elsewhere [43, 47].

The respective specific capacitance evaluated from the voltammetric charge and the useful potential windows of the cyclic voltammogram (Fig. 2) are given in Table 1. The specific capacitance (C(i) where (i) is either an oxide or activated carbon) of the different compounds follows the order $C(V_2O_5) > C(MnO_2) > C(\text{activated carbon}) > C(Fe_3O_4)$ in

Compound	BET (m^2/g)	XRD	Useful potential window (V vs. Ag/AgCl)	Specific capacitance[a] (F/g)
MnO_2	200± 10	amorphous	0.0/1.0	150±8
Fe_3O_4	200± 10	magnetite	−0.7/0.2	75±4
V_2O_5	NM[b]	amorphous	−0.2/1.0	170±9
Activated carbon	2800±100	-	−1.3/0.8	130±7

[a] Evaluated by cyclic voltammetry (See Experimental Section for details)
[b] Not measured

TABLE 1 Physical and electrochemical properties of various active electrode materials

0.1 M K_2SO_4. This trend is in good agreement with the data already published for composite electrodes. Indeed, the larger specific capacitance of V_2O_5 compared to MnO_2 is in agreement with the data reported by Goodenough et al. for these two oxides [12, 46]. The superior capacitance of MnO_2 with respect to Fe_3O_4 has been previously pointed out by Brousse and Bélanger [28]. However, higher capacitance values (> 500 F/g) have been reported for MnO_2 thin films and can be explained by the fact that a larger fraction of the electrode materials is electrochemically active compared to the composite electrode where only a very thin layer is involved in the charge storage process [30]. Unfortunately, the specific capacitance of the V_2O_5 electrode, which is the highest when the initial values are considered, exhibits a quick fade over only a few hundred cycles [47]. Since electrochemical capacitors require long-term stability of the active electrode materials, V_2O_5 was not tested in a two-terminal capacitor in this study.

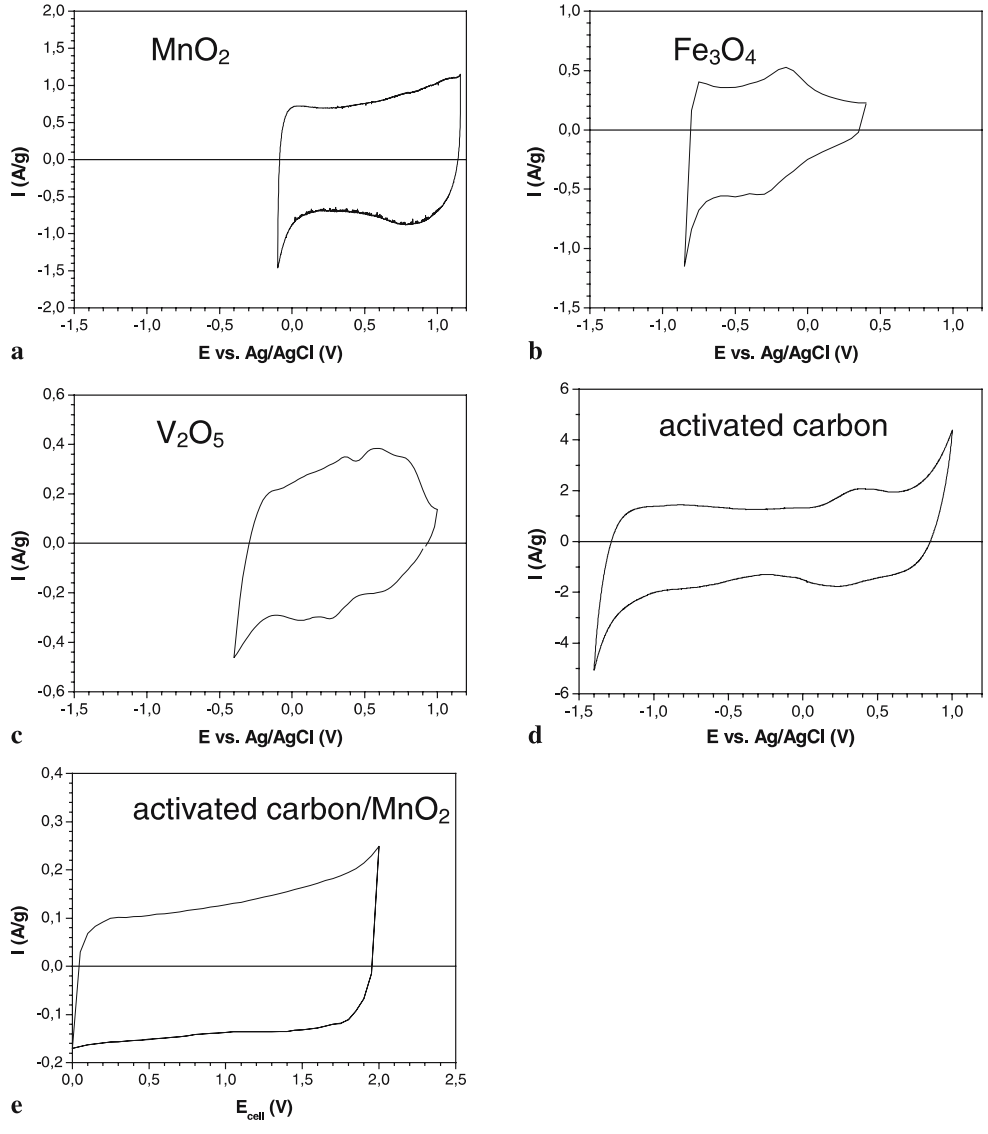

FIGURE 2 Cyclic voltammograms (CV) of composite electrodes in 0.1 M K_2SO_4 (**a**) MnO_2 at a rate of 5 mV/s, (**b**) Fe_3O_4 at a rate of 5 mV/s, (**c**) V_2O_5 at a rate of 2 mV/s, (**d**) activated carbon at a rate of 10 mV/s, (**e**) hybrid device (activated carbon/MnO_2) at a rate of 2 mV/s

3.3 *Charge/discharge curves*

Based on the cyclic voltammogram, it is clear that MnO_2 presents the highest capacitance in 0.1 M K_2SO_4. Subsequently, a symmetric device was assembled, using two MnO_2 electrodes. Despite an interesting galvanostatic charge/discharge cycling behavior (Fig. 3, curve (a)), the energy and power densities are limited due to restricted cell voltage (1 V as a maximum). A calculation of the energy and power densities based on (2) and (3) gives 3.3 Wh/kg and 0.265 kW/kg, respectively. The same remark applies to a symmetric Fe_3O_4/Fe_3O_4 supercapacitor in 0.1 M K_2SO_4 (not shown), which developed a lower cell voltage of only 0.6 V. In this case the energy and power densities are even more limited than for the MnO_2/MnO_2 supercapacitor since both the capacitance and the cell potential are smaller than those of MnO_2.

In order to increase the energy and power densities of oxide-based electrochemical capacitors, it was envisioned to associate a positive MnO_2 electrode with a negative electrode that could increase the cell potential while keeping a reasonable capacitance [28, 29, 49]. A quick look at the cycling voltammograms of Fig. 2 reveals that this could be achieved with two systems: a manganese dioxide electrode can be associated either to an activated carbon electrode [29, 49] or to a Fe_3O_4 electrode [28]. These two asymmetric devices were built and for these capacitors, the weight of the negative and positive electrodes were determined by taking into account the specific voltammetric charge and the appropriate useful potential windows of each materials. As a representative example, the CV of a hybrid activated carbon/MnO_2 device is presented in Fig. 2e. As expected, the electrochemical window is greatly enhanced by associating these two different electrodes in a cell. The cell potential can extend up to more than 2 V (Fig. 2e) as an effect of the high hydrogen and oxygen evolution overpotential for the carbon (see Fig. 2d) and the MnO_2 electrodes (see Fig. 2a), respectively.

The performance of hybrid devices upon galvanostatic charge/discharge cycling have been compared to symmetric MnO_2/MnO_2 capacitor in aqueous 0.1 M K_2SO_4 (Fig. 3 and Table 2). All three devices exhibit galvanostatic charge–discharge curves which resemble those of electrochemical double layer capacitor. However, a closer look indicates that the slopes of the three systems slightly differ from linearity as a result of the pseudo-Faradaic processes for the oxide electrodes. This trend is more pronounced for the device using two oxide electrodes, namely Fe_3O_4 and MnO_2 (Fig. 3, curve (b)).

As expected, the lowest cell voltage is obtained from the symmetric MnO_2/MnO_2 device (Fig. 2a), which is limited to 1 V. Due to the larger useful electrochemical potential window of activated carbon (AC), the hybrid AC/MnO_2 device exhibits a higher cell voltage (2.2 V, see Fig. 3, curve (c)) than the Fe_3O_4/MnO_2 hybrid device (1.8 V, Fig. 3, curve (b)). However, the symmetric device exhibits the highest capacitance (36.0 F/g, see Table 2), which was expected from the capacitance values of the different oxides reported in Table 1, since MnO_2 has superior performance compared to activated carbon or Fe_3O_4. This last compound used as the negative electrode in a Fe_3O_4/MnO_2 hybrid cell has the lowest capacitance, and subsequently the capacitance of the corresponding hybrid device (21.5 F/g) is 30% less than the capacitance of the activated carbon/MnO_2 system (31.0 F/g). This value is 19% less than for the symmetric device, with, however, the substantial advantage of an enhanced cell potential which is more than twice that of the MnO_2/MnO_2 device.

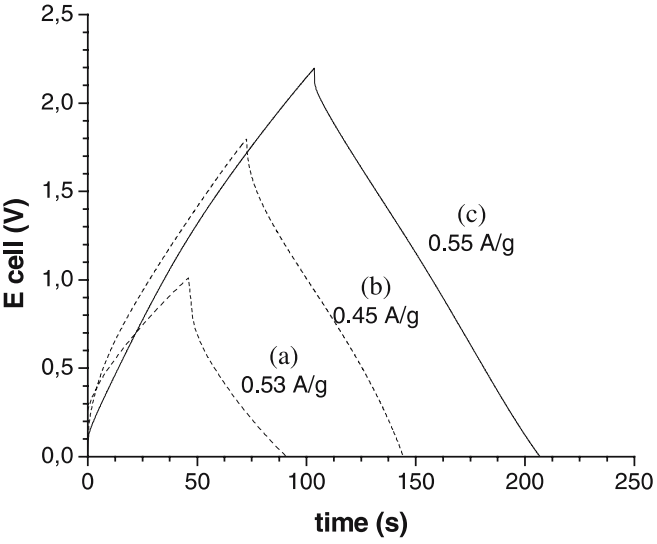

FIGURE 3 Galvanostatic charge/discharge cycles of the different electrochemical capacitors in K_2SO_4: (a) MnO_2/MnO_2, (b) Fe_3O_4/MnO_2, (c) activated carbon/MnO_2

From the galvanostatic curves (Fig. 3), the real energy and power densities were calculated (Table 2). The improvement of cell voltage due to the preparation of hybrid devices (Fe_3O_4/MnO_2 and activated carbon/MnO_2 systems) leads to higher energy and power densities compared to the symmetric MnO_2/MnO_2 supercapacitor, with an increase of 128% in the real power density. The most significant improvement is observed for the real energy density. The activated carbon/MnO_2 hybrid system exhibits an increase of 424% compared to the standard symmetric capacitor. The maximum power density is also greatly enhanced with values as high as 10.2 kW/kg for the Fe_3O_4/MnO_2 system and up to 19 kW/kg for the activated carbon/MnO_2 capacitor.

All these results show that hybrid aqueous systems can be designed with a MnO_2 positive electrode and either a Fe_3O_4

Negative electrode	Positive electrode	Cell voltage (V)	Capacitance F/g[a]	I A/g[a]	P_{real} W/kg[a]	E_{real} Wh/kg[a]	P_{max} W/kg[a]
MnO_2	MnO_2	0–1.0 V	36.0	0.53	265	3.3	3080
Fe_3O_4	MnO_2	0–1.8 V	21.5	0.45	405	8.1	10200
Carbon	MnO_2	0–2.2 V	31.0	0.55	605	17.3	19000

[a] Total weight of active material in the negative and the positive electrodes

TABLE 2 Electrochemical performance of various supercapacitors in 0.1 M K_2SO_4

or activated carbon negative electrode. A very significant enhancement of the energy and power densities have been demonstrated in comparison to standard symmetric MnO_2 devices.

3.4 *Cycling behavior of the hybrid electrochemical supercapacitors*

In order to further characterize the different electrochemical capacitors, their stability upon cycling was investigated under constant cycling power. Fig. 4 demonstrates again that the best performance can be achieved with the hybrid activated carbon/MnO_2 supercapacitor. However, for the two devices, the energy density monotonously fades during the first 5000 cycles. The origin of this energy fade upon cycling is related to the useful electrochemical potential windows of each electrode materials. According to the cyclic voltammograms presented in Fig. 2, it is important to restrict the potential window in order to avoid irreversible processes that could occur if the potential reaches too positive or negative values. Such electrochemical reactions can lead to the dissolution of the active electrode materials in the electrolyte and subsequently causes a decrease in the capacitance due to the loss of active material. This is probably what is occurring for the different oxide based supercapacitors presented in Fig. 4. In fact the low potential limit of MnO_2 must be carefully controlled and monitored and must not go below 0 V vs. Ag/AgCl in order to avoid Mn^{2+} dissolution. If the potential of the positive electrode is more negative than 0 V vs. Ag/AgCl at the end of the cell discharge, then manganese dissolution occurs, leading to a loss of active material from the MnO_2 electrode and subsequently to a loss of capacitance during every cycle as is observed in Fig. 4. This phenomena can be even more pronounced for the Fe_3O_4/MnO_2 capacitor, for which not only the lower potential limit of the positive electrode must be controlled during the discharge but also the lower potential limit of the negative Fe_3O_4 electrode must not decrease below −0.7 V vs. Ag/AgCl during the charge of the capacitor in order prevent the reduction of Fe^{III}. Indeed, the energy density loss upon cycling is more severe in the case of the Fe_3O_4/MnO_2 device for which care must be taken to both electrodes compared to the activated carbon/MnO_2 cell where the activated carbon electrode is less sensitive to excursion to negative potential limits. This can be seen on the slope of the energy density fade which is twice as more important for the Fe_3O_4/MnO_2 device at a constant power cycling of 0.82 kW/kg as for the activated carbon/MnO_2 cell (Fig. 4) at 1.2 kW/kg.

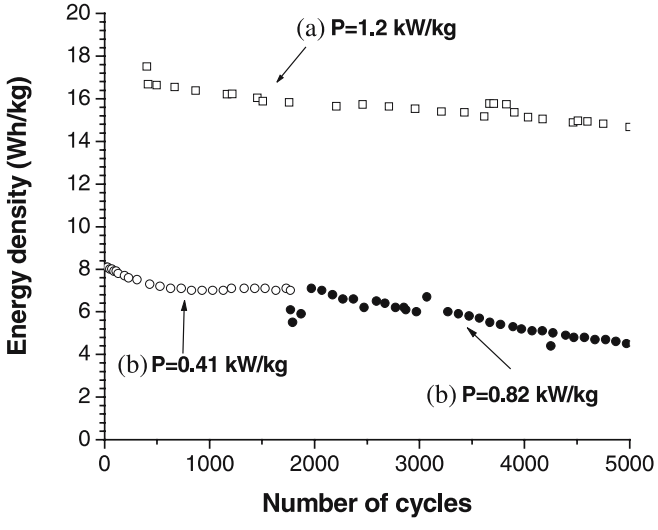

FIGURE 4 Variation of the energy density with the number of cycles for different electrochemical capacitors in K_2SO_4: (a) activated carbon/MnO_2 (cut-off voltage = 2.2 V), (b) Fe_3O_4/MnO_2 (cut-off voltage = 1.8 V). For clarity, only the data obtained at constant power density are presented even if the capacitor was submitted to different power discharge regimes during the charge/discharge tests

From a practical point of view, it means that the weights of the positive and negative electrodes have to be carefully balanced so that each electrode is strictly maintained within its safe electrochemical window during the charge/discharge cycles. This has been recently demonstrated for carbon/conducting polymer electrochemical capacitors [53]. To reach an appropriate capacitance balance, the hybrid activated carbon/MnO_2 supercapacitor is more suitable since the carbon negative electrode is much less potential sensitive (within the electrochemical window used here). Despite this energy fade, a value of 15 Wh/kg is still measured following 5000 cycles at a constant power of 1.2 kW/kg for the activated carbon/MnO_2 capacitor. These are quite promising values for a laboratory cell, working in K_2SO_4 neutral aqueous media.

Thus, the activated carbon/MnO_2 hybrid device appears superior to the Fe_3O_4/MnO_2 capacitor. However, this last system makes use of two simple oxides and avoids the utilization of activated carbon electrode, which can be interesting for low cost devices. Additionally, the smaller cell voltage (1.8 V compared to 2.2 V for activated carbon/MnO_2 cell) can help to limit the hydrogen evolution reaction upon overcharge. Subsequently, the Fe_3O_4/MnO_2 can find applications if the capacitance of the negative electrode is further optimized.

As previously mentioned, the CVs of the activated carbon and MnO_2 electrode have shown the potential limits out of which gas evolution will occur to a non negligible extent, and practically restrict the cell voltage to a maximum of 2.2 V. Subsequently, it seems useful to determine the sensitivity of the activated carbon/MnO_2 capacitor upon accidental overcharge.

3.5 *Overcharging the hybrid activated* carbon/ MnO_2 *supercapacitor*

As previously mentioned, potential limits are of great importance for both electrodes of the activated carbon/MnO_2 cell. Subsequently, it is thought that the hybrid cell should be very sensitive to overcharging. The same cell was charged at increasing voltages between 2.2 and 2.7 V (Fig. 5a). Above a limit of 2.75 V, the system cannot be charged any longer and vigorous gas evolution takes place. However, below this limit, the Coulombic efficiency is very good even at very high voltage (e.g., 97% at 2.7 V). The effects of overcharging the cell are more obvious on the cyclability of the cell. For each charge voltage, the first and the tenth cycles have been plotted (Fig. 5b). One can see that above 2.5 V, the charge/discharge time decreases upon cycling, and subsequently the energy density gets lower at each

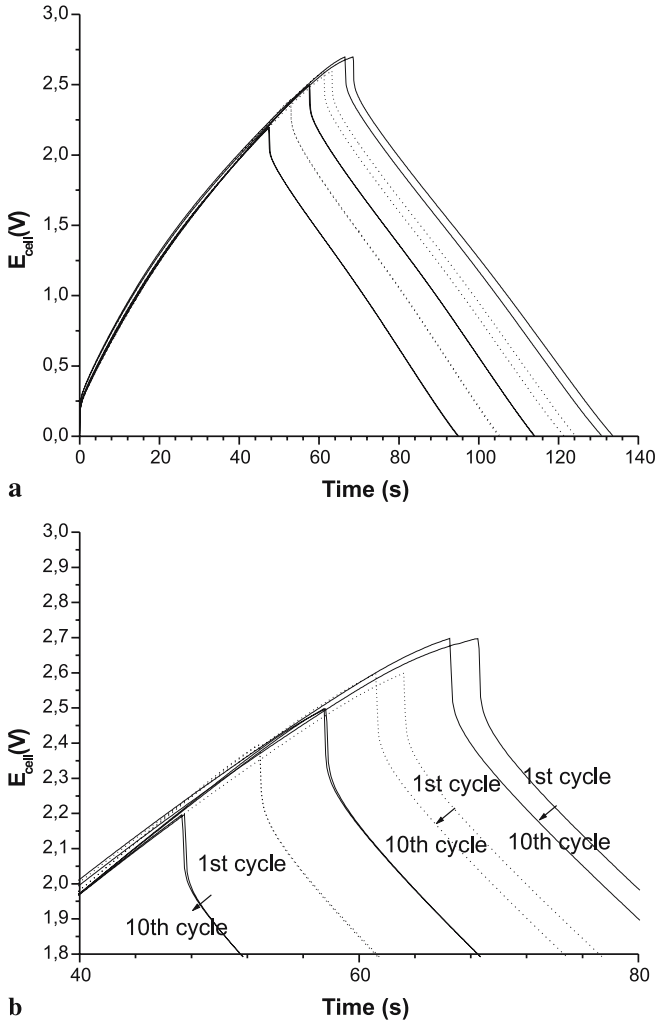

FIGURE 5 Galvanostatic charge/discharge cycles of (**a**) the activated carbon/MnO_2 hybrid cell in K_2SO_4 at different upper cut-off voltage, 2.2 V, 2.4 V, 2.5 V, 2.6 V, 2.7 V; (**b**) zoom of the charge at potential above 1.8 V

cycle under constant power cycling. This trend is confirmed when prolonged cycling is performed.

Obviously, there is a slight negative effect of repeatedly overcharging the cell above 2.5 V, but these tests reveal that the hybrid system can be charged up to 2.7 V. Other safety and practical concerns have to be addressed (e.g., volume of gas generated upon overcharging and self-discharge behavior), but the aqueous activated carbon/MnO_2 hybrid capacitor has already demonstrated promising performance for the development of environmentally friendly low cost devices.

4 Conclusion

Different transition metal oxides, namely MnO_2, Fe_3O_4 or V_2O_5, have been investigated as possible electrodes for electrochemical supercapacitors working in neutral aqueous media such as 0.1 M K_2SO_4. MnO_2 and V_2O_5 exhibit interesting specific capacitance values of 150 and 170 F/g respectively. A smaller value is measured for Fe_3O_4 (75 F/g). However only MnO_2 and Fe_3O_4 maintained a good specific capacitance after 1000 cycles, while the capacitance of V_2O_5 based electrode drastically fades after only a few hundred cycles. A MnO_2 positive electrode was associated with different negative electrodes (MnO_2, activated carbon, Fe_3O_4) in order to build electrochemical supercapacitors. The performance of the symmetric device (MnO_2/MnO_2) is inferior to those of the hybrid devices (activated carbon/MnO_2 and Fe_3O_4/MnO_2). Despite a fade in energy density, the two latter capacitors demonstrate interesting performance over 5000 cycles, especially the activated carbon/MnO_2 device which exhibits a value of 15 Wh/kg at a constant power of 1.2 kW/kg in K_2SO_4 neutral aqueous media.

ACKNOWLEDGEMENTS The financial support of the Natural Science and Engineering Research Council (NSERC) and the Canadian Foundation for Innovation (CFI) is acknowledged. One of the authors (TB) would like to thank "l'Université de Nantes" for giving him the opportunity to work in UQAM, and UQAM for welcoming him as a visiting professor. French Ministère des Affaires Etrangères and Ministère des Relations Internationales du Québec are also greatly acknowledged for supporting this work within the framework of the "Commission Permanente de Coopération Franco-Québécoise" (project #59-102). Part of this work was also supported by MENRT/DGA/CNRS (CAPRYS project PR6-2, ACI Energie 2003). Many thanks to Olivier Crosnier and Romain Dugas for their help with the electrochemical tests.

REFERENCES

1 B.E. Conway, *Electrochemical Supercapacitors, Scientific Fundamentals and Technological Applications* (Kluwer Academic/Plenum Press, New York 1999)
2 P.L. Taberna, P. Simon, J.F. Fauvarque, J. Electrochem. Soc. **150**, A292 (2003).
3 M. Toupin, D. Bélanger, I.R. Hill, D. Quinn, J. Power Sources **140**, 203 (2005)
4 E. Lust, A. Janes, M. Arulepp, J. Electroanal. Chem. **562**, 33 (2004)
5 C. Vix-Guterl, S. Saadallah, K. Jurewicz, E. Frackowiak, M. Redam, J. Parmentier, J. Patarin, F. Béguin, Mater. Sci. Eng. B **108**, 148 (2004)
6 A. Rudge, J. Davey, I. Raistrick, S. Gottesfeld, J.P. Ferraris, J. Power Sources **47**, 89 (1994)
7 F. Fusalba, N. El Mehdi, L. Breau, D. Bélanger, Chem. Mater. **11**, 2743 (1999)
8 E. Naudin, H.A. Ho, S. Branchaud, L. Breau, D. Bélanger, J. Phys. Chem. B **106**, 10585 (2002)
9 H. Kim, B.N. Popov, J. Power Sources **104**, 52 (2002)
10 K.-H. Chang, C.-C. Hu, J. Electrochem. Soc. **151**, A958 (2004)
11 P. Soudan, J. Gaudet, D. Guay, D. Bélanger, R. Schulz, Chem. Mater. **14**, 1210 (2002)
12 H.Y. Lee, J.B. Goodenough, J. Solid State Chem. **144**, 220 (1999); H.Y. Lee, V. Manivannan, J.B. Goodenough, C. R. Acad. Sci. Paris **2** (série II c), 565 (1999)
13 M.S. Wu, P.C.J. Chiang, Electrochem. Solid-State Lett. **7**, A122 (2004)
14 S.C. Pang, M.A. Anderson, T.W. Chapman, J. Electrochem. Soc. **147**, 444 (2000)
15 H.Y. Lee, S.W. Kim, H.Y. Lee, Electrochem. Solid-State Lett. **4**, A19 (2001)
16 C.C. Hu, T.W. Tsou, Electrochem. Comm. **4**, 105 (2002)
17 S.F. Chin, S.C. Pang, M.A. Anderson, J. Electrochem. Soc. **149**, A379 (2002)
18 J. Jiang, A. Kucernak, Electrochim. Acta **47**, 2381 (2002)
19 C.C. Hu, T.W. Tsou, Electrochim. Acta **47**, 3523 (2002)
20 Y.U. Jeong, A. Manthiram, J. Electrochem. Soc. **149**, A1419 (2002)
21 J.N. Broughton, M.J. Brett, Electrochem. Solid-State Lett. **5**, A279 (2002)
22 M.S. Hong, S.H. Lee, S.W. Kim, Electrochem. Solid-State Lett. **5**, A227 (2002).
23 M. Toupin, T. Brousse, D. Bélanger, Chem. Mater. **14**, 3946 (2002)
24 H. Kim, B.N. Popov, J. Electrochem. Soc. **150**, D56 (2003)
25 C.C. Hu, C.-C. Wang, J. Electrochem. Soc. **150**, A1079 (2003)
26 J.K. Chang, W.T. Tsai, J. Electrochem. Soc. **150**, A1333 (2003)
27 R.N. Reddy, R.G. Reddy, J. Power Sources **124**, 330 (2003)

28 T. Brousse, D. Bélanger, Electrochem. Solid State Lett. **6**, A244 (2003)
29 T. Brousse, M. Toupin, D. Bélanger, J. Electrochem. Soc. **151**, A614 (2004)
30 M. Toupin, T. Brousse, D. Bélanger, Chem. Mater. **16**, 3184 (2004)
31 D. Jones, E. Wortham, J. Rozière, F. Favier, J.L. Pascal, L. Monconduit, J. Phys. Chem. Solids **65**, 235 (2004)
32 Y.S. Chen, C.C. Hu, Y.T. Wu, J. Solid State Electrochem. **8**, 467 (2004)
33 Y.K. Zhou, B.L. He, F.B. Zhang, H.L. Li, J. Solid State Electrochem. **8**, 482 (2004)
34 R.N. Reddy, R.G. Reddy, J. Power Sources **132**, 315 (2004)
35 J.K. Chang, Y.L. Chen, W.T. Tsai, J. Power sources **135**, 344 (2004)
36 J.K. Chang, C.T. Lin, W.T. Tsai, Electrochemistry Comm. **6**, 666 (2004)
37 M. Wu, G.A. Snook, G.Z. Chen, D.J. Fray, Electrochemistry Comm. **6**, 499 (2004)
38 J.N. Broughton, M.J. Brett, Electrochim. Acta **49**, 4439 (2004)
39 E. Raymundo-Pinero, V. Khomenko, E. Frackowiak, F. Béguin, J. Electrochem. Soc. **152**, A229 (2005)
40 N.-L. Wu, S.-Y. Wang, C.-Y. Han, D.-S. Wu, L.-R. Shiue, J. Power Sources **113**, 173 (2003)
41 N.L. Wu, Mater. Chem. Phys. **75**, 6 (2002)
42 S.Y. Wang, N.L. Wu, J. Appl. Electrochem. **33**, 345 (2003)
43 T. Cottineau, T. Delahaye, T. Brousse, D. Bélanger, in preparation
44 K.R. Prasad, K. Koga, N. Miura, Chem. Mater. **16**, 1845 (2004)
45 K.R. Prasad, N. Miura, Electrochemistry Comm. **6**, 849 (2004)
46 H.Y. Lee, J.B. Goodenough, J. Solid State Chem. **148**, 81 (1999)
47 T. Cottineau, T. Brousse, D. Bélanger, in preparation
48 M. Pourbaix, N. de Zoubov, *Atlas d'équilibres électrochimiques* (Gautier-Villars, Paris 1963)
49 M.S. Hong, S.H. Lee, S.W. Kim, Electrochem. Solid-State Lett. **5**, A227 (2002)
50 S. Franger, S. Bach, J. Farcy, J.P. Pereira-Ramos, N. Baffier, J. Power Sources **109**, 262 (2002)
51 Z.H. Zhou, J. Wang, X. Liu, J. Mater. Chem. **11**, 1704 (2001)
52 T. Kudo, Y. Ikeda, T. Watanabe, Solid State Ionics **153**, 833 (2002)
53 D. Villers, D. Jobin, C. Soucy, D. Cossement, R. Chahine, L. Breau, D. Bélanger, J. Electrochem. Soc. **150**, A747 (2003)